PHYSICAL REVIEW C **89**, 051602(R) (2014)

Combining *ab initio* calculations and low-energy effective field theory for halo nuclear systems: The case of ^{7}Be + $p \rightarrow {}^8$B + γ

Xilin Zhang, Kenneth M. Nollett, and D. R. Phillips
Institute of Nuclear and Particle Physics and Department of Physics and Astronomy, Ohio University, Athens, Ohio 45701, USA
(Received 24 January 2014; published 8 May 2014)

We report a leading-order (LO) calculation of ^{7}Be$(p,\gamma)^8$B in a low-energy effective field theory. ^8B is treated as a shallow proton+^{7}Be core and proton+^{7}Be* (core excitation) p-wave bound state. The couplings are fixed using measured binding energies and proton-^{7}Be s-wave scattering lengths, together with ^8B asymptotic normalization coefficients from *ab initio* calculations. We obtain a zero-energy S-factor of 18.2 ± 1.2(ANC only) eV b. Given that this is a LO result it is consistent with the recommended value $S(0) = 20.8 \pm 1.6$ eV b. Our computed $S(E)$ compares favorably with experimental data on ^{7}Be$(p,\gamma)^8$B for $E < 0.4$ MeV. We emphasize the important role of proton-^{7}Be scattering parameters in determining the energy dependence of $S(E)$, and demonstrate that their present uncertainties significantly limit attempts to extrapolate these data to stellar energies.

DOI: 10.1103/PhysRevC.89.051602 PACS number(s): 25.40.Lw, 11.10.Ef, 21.10.Jx, 21.60.De

I. INTRODUCTION

The cross section of the reaction ^{7}Be$(p,\gamma)^8$B is important for constraining properties of neutrino oscillations and solar composition through solar-neutrino experiments (e.g., Refs. [1,2]). It must be known at very low ($\sim$20 keV) energies, and this presents a general problem common to nearly all processes in stellar nuclear burning [3]. Such cross sections are very small at these energies because of Coulomb barriers. Most direct measurements have to be carried out at higher energies with larger cross sections and extrapolated down to stellar energies using models.

The accuracy of this approach often suffers from a scarcity of ancillary constraints like elastic cross sections. It also depends on model assumptions regarding, e.g., the number of R-matrix poles or the shape of a potential well. Often the relevance of the constraints to their desired application is doubtful but hard to quantify (as reviewed for ^{7}Be$(p,\gamma)^8$B in Ref. [1]). Recent advances in *ab initio* calculations hold promise to ameliorate the situation [4], but accurate and complete three-nucleon forces are yet to be fully incorporated there [5].

The degrees of freedom and general philosophy of effective field theory (EFT) treatments of such reactions are the same as those in R-matrix and potential-model calculations. EFTs also fix their couplings from particular observables and then predict others. But the EFT's systematic expansion provides a quantitative estimate of the uncertainty at each order of approximation and a framework to improve accuracy. The particular EFT we use here, Halo EFT [6–14], does this by exploiting the separation of energy scales associated with the presence of clusters. Much of a nucleon-level reaction calculation amounts to an indirect treatment of the collective motion of clusters through and around Coulomb and centrifugal barriers, so Halo EFT can profitably be combined with *ab initio* calculations. We extract asymptotic normalization coefficients (ANCs) from *ab initio* eight-body calculations [4,15], combine them with p-^{7}Be scattering lengths from both experiment [16] and theory [4], and perform a predictive Halo EFT computation of ^{7}Be$(p,\gamma)^8$B. This extends Ref. [17]'s calculation of E1 proton capture to the case of a p-wave bound state.

II. ENERGY SCALES AND LAGRANGIAN

It is essential to identify all the pertinent energy scales in this problem (Table I). The presence of a Coulomb barrier generates a low-momentum scale, k_C, associated with its height [14,17,18]. k_C is comparable to the binding momentum of ^8B, γ, which is our generic low-energy scale. The large p-^{7}Be scattering lengths yield two more, quite similar, low-energy scales. All of these generate nonanalytic dependence in the S-factor $S(E)$: if $k = \sqrt{2M_R E}$ then $S = S(k_C/k, ka, k/\gamma)$. We keep the full dependence on these ratios generated by Halo EFT at LO and so have nontrivial analytic structure due to long-wavelength properties of Coulomb wave functions and strong initial-state interactions. This stands in contrast to the Taylor [19–22] expansion sometimes used to describe $S(E)$ around $E = 0$. The EFT's high-energy scale is Λ, the momentum at which ^{7}Be substructure is resolved. $\Lambda \approx 70$ MeV is set by the threshold for $^7\text{Be} \rightarrow {}^3\text{He} + {}^4\text{He}$ and is the radius of convergence in the momentum plane of our result for $S(k)$, which is accurate up to corrections suppressed by γ/Λ. The ^8B ground state is bound by 0.1375 MeV, so $\gamma/\Lambda \approx 0.2$. We use the power counting of Ref. [10] to describe this shallow p-wave bound state: $a_1^{-1} \sim \Lambda\gamma^2$, $r_1 \sim \Lambda$. We also include the core excitation ^{7}Be* as an explicit degree of freedom. Its excitation energy E^* is another low-energy scale.

The Lagrangian we use is $\mathcal{L}_0 + \mathcal{L}_S + \mathcal{L}_P$ (cf. Ref. [23]):

$$\begin{aligned}
\mathcal{L}_0 &= n^{\dagger\sigma}\left(i\partial_t + \frac{\nabla^2}{2M_n}\right)n_\sigma + c^{\dagger a}\left(i\partial_t + \frac{\nabla^2}{2M_c}\right)c_a \\
&\quad + d^{\dagger\delta}\left(i\partial_t + \frac{\nabla^2}{2M_c}\right)d_\delta + \pi^{\dagger\alpha}\left(i\partial_t + \frac{\nabla^2}{2M_{nc}} + \Delta\right)\pi_\alpha, \\
\mathcal{L}_S &= g_{(^3S_1)}c^{\dagger a'}n^{\dagger\sigma'}T^i_{a'\sigma'}T^{a\sigma}_i c_a n_\sigma + g_{(^5S_2)}c^{\dagger a'}n^{\dagger\sigma'}T^\alpha_{a'\sigma'}T^{a\sigma}_\alpha c_a n_\sigma \\
&\quad + g_{(^3S_1^*)}d^{\dagger\delta}n^{\dagger\sigma'}T^i_{\delta\sigma'}T^{a\sigma}_i c_a n_\sigma + \text{C.C.}, \qquad (1) \\
\mathcal{L}_P &= h_{(^3P_2)}\pi^{\dagger\alpha}T^{ij}_\alpha T^{\sigma a}_i n_\sigma i(\boldsymbol{V}_n - \boldsymbol{V}_c)_j c_a \\
&\quad + h_{(^5P_2)}\pi^{\dagger\alpha}T^{\beta j}_\alpha T^{\sigma a}_\beta n_\sigma i(\boldsymbol{V}_n - \boldsymbol{V}_c)_j c_a \\
&\quad + h_{(^3P_2^*)}\pi^{\dagger\alpha}T^{jk}_\alpha T^{\delta\sigma}_k n_\sigma i(\boldsymbol{V}_n - \boldsymbol{V}_{c^*})_j d_\delta + \text{C.C.} \qquad (2)
\end{aligned}$$

TABLE I. Key physical scales in our EFT. The $^8B \to p + {}^7$Be threshold is $B_{^8B}$, the $^7\text{Be} \to {}^3\text{He} + {}^4\text{He}$ threshold is $B_{^7\text{Be}}$, and the ^{7}Be core-excitation energy is E^*. The p-^{7}Be effective mass $M_R \equiv M_n M_c/(M_n + M_c) = 7/8 M_n$ and the ^{3}He-^{4}He effective mass $M'_R = 12/7 M_n$. The scattering parameters a and r in the incoming s-wave channels are not well determined, but generically obey the hierarchy given here. The numbers for a_1 and r_1 are extracted from *ab initio* ANCs.

Momentum scale	Definition	Value
$k_C \sim \gamma$	$Q_c Q_n \alpha_{EM} M_R$	24.02 MeV
γ	$\sqrt{2 M_R B_{^8B}}$	15.04 MeV
Λ	$\sqrt{2 M'_R B_{^7\text{Be}}}$	70 MeV
$\gamma^* \sim \gamma$	$\sqrt{2 M_R (B_{^8B} + E^*)}$	30.53 MeV
$\gamma_\Delta \sim \gamma$	$\sqrt{2 M_R E^*}$	26.57 MeV
$a_{^3S_1}, a_{^5S_2} \sim 1/\gamma$	Scattering lengths	Varies
$r_0 \sim 1/\Lambda$	$l = 0$ effective ranges	Varies
$a_1 \sim \gamma^{-2}\Lambda^{-1}$	Scattering volume	1054.1 fm^3
$r_1 \sim \Lambda$	$l = 1$ effective "range"	-0.34 fm^{-1}

Here n_σ, c_a, d_δ, π_α are fields of the proton ("nucleon"), ^{7}Be core ($\frac{3}{2}^-$), ^{7}Be* ($\frac{1}{2}^-$), and ^8B ground state (2^+), respectively; $g_{(^3S_1)}$ and $g_{(^5S_2)}$ in $\mathcal{L}_S$ are related to "unnaturally" enhanced $\sim 1/\gamma$ s-wave charged-particle scattering lengths (see Refs. [14,17,18]); $g_{(^3S_1^*)}$ describes $^7\text{Be} + p \leftrightarrow {}^7\text{Be}^* + p$ and is assumed to be natural, i.e., $\sim 1/\Lambda$ [23]; and h_Y are the p-wave couplings. The fields' indices are their spin projections with a specific convention: $\sigma,\delta,\sigma',\delta' = \pm 1/2$, $a,a' = \pm 3/2, \pm 1/2$, $\alpha,\beta = \pm 2, \pm 1, 0$, and $i,j,k = \pm 1, 0$; Δ is π^α's bare binding energy; $T^{\cdots}_{\cdots}$s are the C-G coefficients (cf. [23]); $\boldsymbol{V}_{n;c}$ are proton and core velocities. To implement electromagnetic interactions, we use minimal substitution $\partial_\mu \to \partial_\mu + ieQA_\mu$ with $e \equiv \sqrt{4\pi\alpha_{EM}}$ and Q the particle's charge.

III. p-WAVE SCATTERING AND SHALLOW BOUND STATE

We denote π^α's dressed propagator as $D^\beta_\alpha \equiv D\delta^\beta_\alpha$. Its self energy receives contributions from p-^{7}Be intermediate states in the $^3P_2$ and $^5P_2$ channels, and p-^{7}Be* in the $^3P_2$ channel [23]. In each case the proton and ^{7}Be (^{7}Be*) interact via the Coulomb interaction. We include these Coulomb effects to all orders in α_{EM}, thereby extending the calculation of Refs. [14,17,18] to p waves. In practice this involves replacing the plane waves of Ref. [23] by Coulomb wave functions in both external legs and intermediate states. $D(E)$ can then be written in terms of the a_1 and r_1 in the 2^+ channel:

$$\frac{-6\pi M_R}{h_t^2 D} = -\frac{1}{a_1} + \frac{r_1}{2}k^2 - 2k_C\left(k^2 + k_C^2\right)H(k_C/k) - 2k_C\frac{h^2_{(^3P_2^*)}}{h_t^2}\left(k_*^2 + k_C^2\right)H(k_C/k_*). \quad (3)$$

with $H(\eta) = \psi(i\eta) + 1/(2i\eta) - \ln(i\eta)$ [24], $h_t^2 \equiv h^2_{(^3P_2)} + h^2_{(^5P_2)}$, and $k_* \equiv \sqrt{2M_R(E - E^*)}$. a_1 and r_1 are then functions of the Lagrangian parameters $\Delta, h_{(^3P_2)}, h_{(^5P_2)}$, and $h_{(^3P_2^*)}$. If $k < \gamma_\Delta$ we recover the standard Coulomb-modified effective-range expansion for $l = 1$; i.e., the right-hand side of Eq. (3) becomes $C^2_{\eta,1}k^3(\cot\delta_1 - i)$, with δ_1 the phase shift relative to a Coulomb wave, $C_{\eta,l} \equiv 2^l \exp(-\pi\eta/2)|\Gamma(l + 1 + i\eta)|/\Gamma(2l + 2)$, and $\eta \equiv k_C/k$ [25,26].

We write the p-wave Coulomb-distorted T-matrix, T_{CS} [14,26], in the p-^{7}Be-^{7}Be* Hilbert space schematically as $V \times D(E) \times V$. [V stands for n-$c(d)$-π interactions and D is given by Eq. (3).] Since T_{CS} has a pole at $B_{^8B}$ we have $D^{-1}(k = i\gamma) = 0$. The residue then yields a relation for the wave-function renormalization factor, Z:

$$\frac{6\pi}{Z} = -h_t^2 r_1 + 2\frac{k_C}{\gamma}\left\{\frac{h_t^2}{\gamma^2}\left[2\gamma^3\tilde{H}\left(\frac{k_C}{\gamma}\right) + \left(k_C^3 - k_C\gamma^2\right)\tilde{H}'\left(\frac{k_C}{\gamma}\right)\right] + \frac{h^2_{(^3P_2^*)}}{\gamma^{*2}}\left[2\gamma^{*3}\tilde{H}\left(\frac{k_C}{\gamma^*}\right) + \left(k_C^3 - k_C\gamma^{*2}\right)\tilde{H}'\left(\frac{k_C}{\gamma^*}\right)\right]\right\}, \quad (4)$$

where, for convenience, we define $\tilde{H}(z) \equiv H(-iz)$, $\tilde{H}'(z) \equiv d\tilde{H}(z)/dz$. The $^8B \to p + {}^7\text{Be}(^7\text{Be}^*)$ ANCs, $C_{(^5P_2)}$, $C_{(^3P_2)}$, and $C_{(^3P_2^*)}$ are then given by (cf. Ref. [23])

$$\frac{C^2_{(Y)}}{h_Y^2\gamma^2\Gamma^2(2 + k_C/\gamma)} = \frac{C^2_{(^3P_2^*)}}{h^2_{(^3P_2^*)}\gamma^{*2}\Gamma^2(2 + k_C/\gamma^*)} = \frac{Z}{3\pi}, \quad (5)$$

with $Y = {}^3P_2$ and $^5P_2$.

IV. LEADING-ORDER PROTON CAPTURE

The relevant diagrams are shown in Fig. 1. Let us first focus on initial total spin $S_i = 1$ and use the notation, $\langle\pi^\alpha|L_{\text{EM}}|\chi^{(+)}_{\boldsymbol{p}},\delta,a\rangle \equiv T_i^{\delta a}T_\alpha^{ij}\mathcal{M}_j$, with L_{EM} the term in the Lagrangian that governs the interaction with the (transverse) photon, $\boldsymbol{j}_{\text{EM}} \cdot \boldsymbol{A}$, and $|\chi^{(+)}_{\boldsymbol{p}},\delta,a\rangle$ the incoming Coulomb wave function for the p-^{7}Be state, labeled by the asymptotic relative momentum $\boldsymbol{p}$ and the individual spin projections of the two particles. The LO $\mathcal{M}_j$ is computed in coordinate space and decomposed into contributions from incoming s and

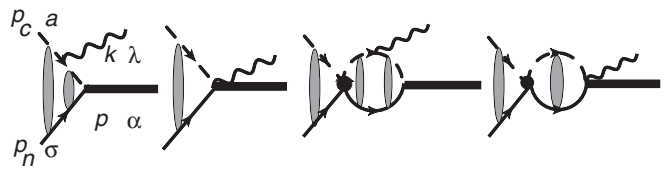

FIG. 1. Diagrams for capture. The line assignments are designated by the spin indices; the shaded blobs denote the full Coulomb-Green functions; the bold vertex in the last two diagrams means S-wave multiple scattering with the Coulomb interaction included to all orders in α_{EM} [18,23]. Diagrams with the photon coupled to the proton are not shown but are included in our calculation.

d waves:

$$\mathcal{M}_j = (-i)C_{\eta,0}C^{\rm LO}_{(^3P_2)}\frac{Z_{\rm eff}}{M_R}\frac{2\pi}{\sqrt{3}}(\gamma^2+k^2)$$
$$\times\left[e^{i\sigma_0}\epsilon^*_j(\lambda)Y_{00}(\hat{\mathbf{p}})\mathcal{S}(^3S_1)\right.$$
$$\left.+\,e^{i\sigma_2}\epsilon^*_k(\lambda)\sqrt{2}T_j^{k\beta}Y_{2\beta}(\hat{\mathbf{p}})\mathcal{D}\right],$$
$$\mathcal{S}(X)\equiv\int_0^{+\infty}dr\,W_{-\eta_B,\frac{3}{2}}(2\gamma r)r\left[\frac{C_{\eta,0}G_0(k,r)}{-a^{-1}_{(X)}-2k_CH(\eta)}\right.$$
$$\left.+\,\frac{F_0(k,r)}{C_{\eta,0}k}\frac{-a^{-1}_{(X)}-2k_C{\rm Re}[H(\eta)]}{-a^{-1}_{(X)}-2k_CH(\eta)}\right],$$
$$\mathcal{D}\equiv\int_0^{+\infty}dr\,W_{-\eta_B,\frac{3}{2}}(2\gamma r)r\frac{F_2(k,r)}{C_{\eta,0}k}. \qquad (6)$$

Here, $C^{\rm LO}_{(^3P_2)}$ is the LO ANC (see below); $Z_{\rm eff}/M_R\equiv eQ_n/M_n-eQ_c/M_c$; $\epsilon^*(\lambda)$ is the photon polarization (λ) vector. σ_l is the Coulomb phase shift; F_l and G_l are Coulomb wave functions for angular momentum l, and $W_{-\eta_B,\frac{3}{2}}$ is a Whittaker function with $\eta_B\equiv k_C/\gamma$ [25]. Proceeding similarly with $S_i=2$ we obtain the same result but with $[C^{\rm LO}_{(^3P_2)},a_{(^3S_1)}]\to[C^{\rm LO}_{(^5P_2)},a_{(^5S_2)}]$. The s-wave scattering lengths, $a_{(^3S_1)}$ and $a_{(^5S_2)}$, describe LO incoming channel multiple scattering (ICMS) effects. We thus obtain the S factor, including all initial channels:

$$S(E)=\frac{e^{2\pi\eta}}{e^{2\pi\eta}-1}\frac{Z^2_{\rm eff}}{M_R^2}\frac{\pi}{24}\omega k_C(\gamma^2+k^2)^2$$
$$\times\frac{5}{3}\left[{C^{\rm LO}_{(^3P_2)}}^2(|\mathcal{S}(^3S_1)|^2+2|\mathcal{D}|^2)\right.$$
$$\left.+\,{C^{\rm LO}_{(^5P_2)}}^2(|\mathcal{S}(^5S_2)|^2+2|\mathcal{D}|^2)\right]. \qquad (7)$$

V. RESULTS

Table II collects information on $^8B\to{}^7{\rm Be}+p$ ANCs and p-^{7}Be scattering lengths. The *ab initio* ANCs of Nollett and Wiringa were computed using variational Monte Carlo with the Argonne $v18$ + Urbana IX Hamiltonian [27,28], which includes three-nucleon terms. They are consistent with those from the experiment in Ref. [29] and may have smaller errors (though errors reported for the calculation account only for Monte Carlo sampling). These ANCs are also consistent with *ab initio* ANCs found from an SRG-N^{2}LO two-body interaction in the RGM-NCSM approach by Navratil *et al.* [4]. We extended the calculations in Ref. [15] to include the $^8B\to{}^7{\rm Be}^*+p$ ANC, $C_{(^3P^*_2)}=-0.3485(51){\rm fm}^{-1/2}$.

Using the Nollett ANCs, the ^{8}B binding energy, and Eqs. (5) and (4), we obtain the results for a_1 and r_1 shown in Table I—values that conform to the scaling assigned to a_1 and r_1. If $r_1\sim\Lambda$ then the first term on the right-hand side of Eq. (4) dominates over the second one. We therefore use the full Eq. (4), together with Eq. (5), to extract the value of r_1, but then define "LO ANCs," via

$$\frac{\left[C^{\rm LO}_{(Y)}\right]^2}{h_Y^2\gamma^2\Gamma^2(2+k_C/\gamma)}=\frac{\left[C^{\rm LO}_{(^3P^*_2)}\right]^2}{h^2_{(^3P^*_2)}\gamma^{*2}\Gamma^2(2+k_C/\gamma^*)}=-\frac{2}{h_t^2r_1}. \qquad (8)$$

This yields ${C^{\rm LO}_{(\cdots)}}^2/C^2_{(\cdots)}=Z^{\rm LO}/Z=0.87$; i.e., after obtaining an input value for r_1 from the *ab initio* calculation, we drop terms that are higher order in the γ/Λ expansion in the EFT expression for the ANCs. This is an extension of the ρ-parameterization of s-wave EFT couplings defined in Ref. [30] to the p-wave case. The difference between the ρ-parameterization and the Z-parameterization (the use of which would correspond here to employing the full ANCs at leading order) is higher order. A number of EFT results in the two-body sector (including those of Ref. [23], which are directly relevant to this application) show that the ρ-parametrization leads to smoother convergence for EFT observables than does the Z-parameterization; it builds up the full ANC order-by-order in the γ/Λ expansion. This is especially advantageous in applications where peripheral capture and mechanisms that are operative at distances $r\sim1/\Lambda$ contribute to the matrix element with opposite sign. Consequently, to compute our LO E1 result for the S factor in $^7{\rm Be}(p,\gamma)^8$B we insert the LO ANCs defined by Eq. (8) into Eq. (7).

At low energies, $E<0.1$ MeV, a quadratic approximation $S(E)=S(0)(1+d_1E+d_2E^2)$ is customary [20–22]. Table III lists results, based on different inputs, for the full $S(0)$, the S_i=1 channel contribution $S_{(^3S_1)}(0)$, d_1, and d_2. The peripheral nature of the capture in this regime means both the $S_i=1$ and $S_i=2$ contributions to $S(0)$ depend only very weakly on ICMS—as seen in Refs. [20–22]. As a result, $S_{(^3S_1)}(0)$ and $S_{(^5S_2)}(0)$ essentially both scale with their corresponding LO ANCs. The recommended value of Ref. [1]

TABLE II. Input parameters. "Nollett" [15] and "Navratil" [4] are *ab initio* results, while "Tabacaru" [29] and "Angulo" [16] are from experiment. The "Tabacaru" ANCs have been transformed into the spin-coupled basis assuming the relative signs found in the *ab initio* calculations of Ref. [15]. The units are fm$^{-1/2}$ and fm for ANCs and scattering lengths, respectively.

	$C_{(^3P_2)}$	$C_{(^5P_2)}$	$a_{(^3S_1)}$	$a_{(^5S_2)}$
Nollett	−0.315(19)	−0.662(19)		
Navratil	−0.294	−0.650	−5.2	−15.3
Tabacaru	0.294(45)	0.615(45)		
Angulo			25(9)	−7(3)

TABLE III. Results for Taylor-expansion coefficients. No + A, Na, and T + A are the results from using "Nollett" + "Angulo", "Navratil", and "Tabacaru" + "Angulo" inputs listed in Table II. The uncertainties in No + A and T + A entries are due to ANC uncertainties listed in Table II. Recommended values from Ref. [1] are shown for comparison.

	$S(0)$ (eV b)	$S_{(^3S_1)}(0)$	d_1(MeV^{-1})	d_2 (MeV^{-2})
No + A	18.2 ± 1.2	3.1 ± 0.4	−1.62	10.3
Na	17.8	3.0	−1.26	10.8
T + A	15.7 ± 2.7	2.7 ± 0.8	−1.62	10.3
Ref. [1]	20.8 ± 1.6		−1.5 ± 0.1	6.5 ± 2.0

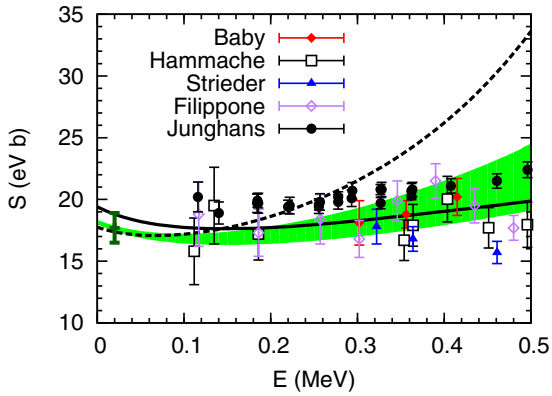

FIG. 2. (Color online) $E1$ S factor for proton capture on ^{7}Be. The green shaded band is the range of $S(E)$ in the LO calculation with "No + A" input (cf. Table III), varying scattering lengths within their 1σ errors. The (nearly energy-independent) impact of the ANC error bar on the prediction is indicated by the error bar on the "No + A" band at 20 keV. The data are from Refs. [32–35]. The solid black curve is the NCSM/RGM calculation of Ref. [4], shown for comparison with its LO EFT approximation (dashed), computed using the "Na" parameters given in Table III.

for $S(0)$, which was fitted to direct capture data using a model, is consistent with our $S(0)$ within uncertainties (including the higher-order EFT uncertainty of $\approx 10\%$, see below). The d_1 and d_2 of Ref. [1] were obtained by fitting quadratics to model curves (not data) in the range $0 \leqslant E \leqslant 50$ keV; we define our coefficients in the same way and find consistent results, though our d_2 are near the high end of a large variation among models. Exact derivatives computed at threshold are in close agreement with potential models [31].

In Fig. 2 we show the LO Halo EFT prediction for $S(E)$ obtained from the "Nollet" ANCs and the 1σ range of experimental scattering lengths [16]. The errors on the ANCs smear out the prediction by an additional $\sim$10% at all energies as shown by an error bar at 20 keV. In contrast, the impact of scattering length uncertainties increases dramatically with energy: when $E < 0.1$ MeV, it is <5%, but it reaches 20% at $E \approx 0.4$ MeV. The consequent range of Halo-EFT predictions is consistent with direct capture data for $0.1 \leqslant E \leqslant 0.4$ MeV (below the M1 resonance) and with indirect S factors derived from Coulomb breakup [36–38]. However, the energy dependence seen at the upper edge of the band in Fig. 2 is not consistent with the trend of the data. This rapidly rising $S(E)$ happens because the real part of the denominator in Eq. (6) vanishes at some energy $E_p > 0$ if $a_{(^5S_2)} < 0$. Even though the breakdown energy of our EFT is on the scale of 1 MeV, we do not show $S(E)$ beyond 0.5 MeV because the well-known M1 resonance contribution [1,4] has a significant impact for $E > 0.5$ MeV and the resonant channel is not included in our calculation. We find that in the window $0.1 \leqslant E \leqslant 0.5$ MeV ICMS effects generate appreciable energy dependence in $S(E)$, and the use of scattering lengths at the extremes of the "Angulo" $1\text{-}\sigma$ ranges result in rather different shapes for $S(E)$.

In order to assess the extent to which higher-order terms in the EFT affect this finding we have compared the RGM-NCSM result of Ref. [4] (solid curve) with an EFT calculation that takes the scattering lengths and ANCs found in Ref. [4] as input ("Na" input, dashed curve). Since an all orders EFT calculation with Ref. [4]'s input should reproduce the solid curve exactly, the distance between these two lines is indicative of the size of higher-order effects. (This holds regardless of the fact that Ref. [4]'s *ab initio* calculation did not include three-nucleon forces.) The LO calculation with "Na" input rises significantly faster than the data because E_p is quite small for $a_{(^5S_2)} = -15.3$ fm. It would appear that in Ref. [4] these larger values of the scattering lengths were offset by compensating mechanisms that are higher order in the EFT. We investigate two different candidates for this, both of which appear in the EFT expansion for $S(E)$ at NLO. First, we introduce an effective-range term in the s-wave scattering amplitude. For simplicity we choose the same effective range, r_0, for both channels. Varying r_0 from its LO value of 0 to 2 fm changes the S factor by less than 10%, even when $a_{(^5S_2)} = -15.3$ fm and $E = 0.4$ MeV so that the effect is largest. Second, we change the lower limit of integration, $r_{\rm min}$, in Eq. (6) to estimate the size of higher-order, short-distance effects like the contact operators that enter the capture amplitudes at NLO [23]. With "Na" input and $r_0 = 2$ fm, an $r_{\rm min}$ of 2 fm flattens $S(E)$, reducing it by 10% at 0.4 MeV. Varying parameters by hand, we find that $r_0 = r_{\rm min} = 3$ fm brings the energy dependence of our LO "Na" $S(E)$ curve close to that of the full RGM-NCSM result.

We emphasize that although the precise magnitude and shape of $S(E)$ predicted by Halo EFT will be modified by higher-order contributions, the sensitivity to p-^{7}Be scattering parameters we have diagnosed here should persist. We conclude that it is important to improve the accuracy of s-wave scattering length (and perhaps effective range) measurements in order to constrain the extrapolation of $S(E)$ data to zero energy. This supports similar conclusions from other formalisms [1,36,39]. Models with incorrect scattering lengths get a key nonanalyticity of the low-energy capture amplitude wrong.

VI. SUMMARY

We have applied Halo EFT to radiative proton capture on ^{7}Be. In Halo EFT the short-distance piece of the Coulomb-nuclear interference is entangled with the pure nuclear amplitude, so this process is not straightforwardly connected to radiative neutron capture on ^{7}Li, although isospin symmetry is regularly used to relate the two in models. Discussion of this issue and other details of our calculation will be presented elsewhere [40]. The strategy used here is, however, the same as in Ref. [23]: fix the EFT couplings using *ab initio* ANCs and experimental binding energies and scattering lengths.

Our LO Halo EFT result for $S(0)$ is $\approx$10% below the recommended value [1] but is consistent with it within the combined EFT and ANC uncertainties. The significant uncertainties in the experimental $a_{(^5S_2)}$ and $a_{(^3S_1)}$ mean that the energy dependence of $S(E)$ is not well constrained above 0.1 MeV, although the central values produce a trend that agrees with direct capture data quite well. This shows the importance of improved measurements of p-^{7}Be scattering, which would render the extrapolation of capture data to solar energies more reliable. On the theory side, a next-to-leading-order calculation of $p + {}^7\text{Be} \to {}^8\text{B} + \gamma$ will be important to reduce the EFT

uncertainty and so make Halo EFT competitive as a tool for determining this key input to predictions of solar neutrino fluxes.

ACKNOWLEDGMENTS

X.Z. and D.R.P. acknowledge support from the US Department of Energy under Grant No. DE-FG02-93ER-40756. K.M.N. acknowledges support from the Institute of Nuclear and Particle Physics at Ohio University. We thank Carl Brune for useful comments on the manuscript and Petr Navratil for both his comments and sharing with us the table of his numerical results.

[1] E. G. Adelberger *et al.*, Rev. Mod. Phys. **83**, 195 (2011).
[2] W. C. Haxton, R. G. H. Robertson, and A. M. Serenelli, Ann. Rev. Astron. Astrophys. **51**, 21 (2013).
[3] C. E. Rolfs and W. S. Rodney, *Cauldrons in the Cosmos: Nuclear Astrophysics* (University of Chicago Press, Chicago, 1988).
[4] P. Navratil, R. Roth, and S. Quaglioni, Phys. Lett. B **704**, 379 (2011).
[5] G. Hupin, J. Langhammer, P. Navrátil, S. Quaglioni, A. Calci, and R. Roth, Phys. Rev. C **88**, 054622 (2013).
[6] U. van Kolck, Nucl. Phys. A **645**, 273 (1999).
[7] D. B. Kaplan, M. J. Savage, and M. B. Wise, Phys. Lett. B **424**, 390 (1998).
[8] D. B. Kaplan, M. J. Savage, and M. B. Wise, Nucl. Phys. B **534**, 329 (1998).
[9] C. A. Bertulani, H.-W. Hammer, and U. Van Kolck, Nucl. Phys. A **712**, 37 (2002).
[10] P. F. Bedaque, H.-W. Hammer, and U. van Kolck, Phys. Lett. B **569**, 159 (2003).
[11] H.-W. Hammer and D. R. Phillips, Nucl. Phys. A **865**, 17 (2011).
[12] G. Rupak and R. Higa, Phys. Rev. Lett. **106**, 222501 (2011).
[13] D. L. Canham and H.-W. Hammer, Eur. Phys. J. A **37**, 367 (2008).
[14] R. Higa, H.-W. Hammer, and U. van Kolck, Nucl. Phys. A **809**, 171 (2008).
[15] K. M. Nollett and R. B. Wiringa, Phys. Rev. C **83**, 041001 (2011).
[16] C. Angulo *et al.*, Nucl. Phys. A **716**, 211 (2003).
[17] E. Ryberg, C. Forssén, H.-W. Hammer, and L. Platter, Phys. Rev. C **89**, 014325 (2014).
[18] X. Kong and F. Ravndal, Phys. Lett. B **450**, 320 (1999); Nucl. Phys. A **665**, 137 (2000).
[19] R. D. Williams and S. E. Koonin, Phys. Rev. C **23**, 2773 (1981).
[20] D. Baye and E. Brainis, Phys. Rev. C **61**, 025801 (2000).
[21] D. Baye, Phys. Rev. C **62**, 065803 (2000).
[22] D. Baye, Nucl. Phys. A **758**, 114 (2005).
[23] X. Zhang, K. M. Nollett, and D. R. Phillips, Phys. Rev. C **89**, 024613 (2014).
[24] M. Abramowitz and I. A. Stegun, eds., *Handbook of Mathematical Functions* (Dover Publications, New York, 1972).
[25] M. L. Goldberger and K. M. Watson, *Collision Theory* (Wiley, New York, 1964).
[26] S. Koenig, D. Lee, and H.-W. Hammer, J. Phys. G: Nucl. Part. Phys. **40**, 045106 (2013).
[27] R. B. Wiringa, V. G. J. Stoks, and R. Schiavilla, Phys. Rev. C **51**, 38 (1995).
[28] B. S. Pudliner, V. R. Pandharipande, J. Carlson, and R. B. Wiringa, Phys. Rev. Lett. **74**, 4396 (1995).
[29] G. Tabacaru, A. Azhari, J. Brinkley, V. Burjan, F. Carstoiu, C. Fu, C. A. Gagliardi, V. Kroha *et al.*, Phys. Rev. C **73**, 025808 (2006).
[30] D. R. Phillips, G. Rupak, and M. J. Savage, Phys. Lett. B **473**, 209 (2000).
[31] B. K. Jennings, S. Karataglidis, and T. D. Shoppa, Phys. Rev. C **58**, 3711 (1998).
[32] B. W. Filippone, A. J. Elwyn, C. N. Davids, and D. D. Koetke, Phys. Rev. C **28**, 2222 (1983).
[33] L. T. Baby *et al.* (ISOLDE Collaboration), Phys. Rev. Lett. **90**, 022501 (2003); **92**, 029901(E) (2004).
[34] A. R. Junghans *et al.*, Phys. Rev. C **68**, 065803 (2003).
[35] A. R. Junghans, K. A. Snover, E. C. Mohrmann, E. G. Adelberger, and L. Buchmann, Phys. Rev. C **81**, 012801 (2010).
[36] B. Davids and S. Typel, Phys. Rev. C **68**, 045802 (2003).
[37] F. Schümann *et al.*, Phys. Rev. C **73**, 015806 (2006).
[38] T. Kikuchi *et al.*, Eur. Phys. J. A **3**, 213 (1998).
[39] P. Descouvemont, Phys. Rev. C **70**, 065802 (2004).
[40] X. Zhang, K. Nollett, and D. R. Phillips (unpublished).